UDK 669.14.018.85:669.778:620.193
Izvirni znanstveni članek

ISSN 1580-2949
MATER. TEHNOL. 34(6)331(2000)

ABSORPTION AND DIFFUSION OF HYDROGEN IN STEELS

ABSORPCIJA IN DIFUZIJA VODIKA V JEKLIH

Hans Jürgen Grabke, Ernst Riecke

Max-Planck-Institut für Eisenforschung GmbH, Postfach 140444, 40074 Düsseldorf, Germany

Prejem rokopisa - received: 2000-12-11; sprejem za objavo - accepted for publication: 2000-12-20

To understand and control hydrogen-induced cracking and hydrogen-induced stress-corrosion cracking in steels, the fundamental processes of hydrogen absorption and diffusion are of interest.

The electrochemical hydrogen permeation method has been extensively applied to obtain data on hydrogen absorption and diffusion in iron, iron alloys and steels. Steady-state permeation measurements yield the permeation coefficient and the hydrogen concentration and activity a_H, which are established on the surface in electrolytes. This information was used to study the effects of alloying elements on a_H present during corrosion.

Permeation transients from non-steady-state measurements yield the hydrogen diffusivity, which is affected by the presence of hydrogen traps. For shallow traps with low binding energies a distribution equilibrium between trap and lattice sites applies, deep traps are already saturated at low a_H and hydrogen in deep traps is immobile at ambient temperature. The effects of Mo, V, Nb, Ti, Zr and their carbides and nitrides on the hydrogen diffusivity were studied and information was derived on the numbers and binding energies of traps which are caused by strain fields around big atoms of alloying elements or in the neighbourhood of their precipitates.

For some pipeline steels with different microstructures, and after welding simulation, hydrogen diffusivities and trapping were studied. The results were related to hydrogen-induced stress-corrosion cracking, which was observed in constant-extension-rate tests. The work of fracture decreased with increasing hydrogen activity, i.e. the mobile hydrogen is decisive for failure, and the hydrogen in deep traps has no obvious effect on the fracture behaviour of steels.

Key words: iron alloys, pipeline steels, hydrogen activity, permeation, diffusivity, fracture energy

Za razumevanje in kontrolo pokanja zaradi vodika in napetostnega korozijskega pokanja jekel je treba poznati temeljne procese absorpcije in difuzije vodika.

Metoda elektrokemične permeacije vodika se je mnogo uporabljala za pridobivanje podatkov o absorpciji in difuziji vodika v železu, njegovih zlitinah in jeklih. Iz meritev permeacije v stacionarnem stanju so bili določeni koeficient permeacije ter koncentracija in aktivnost vodika na površini kovine v elektrolitih. Metoda je bila tudi uporabljena za določanje vpliva legirnih elementov na aktivnost vodika med korozijo.

Tranzienti permeacije pri nestacionarnih meritvah dajo podatke o difuzivnosti vodika, na katero vplivajo prisotne pasti. Za plitve pasti z majhno vezno energijo se vzpostavi ravnotežje med pastmi in mrežnimi mesti.

Globoke pasti so nasičene že pri majhni aktivnosti vodika, vodik v njih pa je nepremičen pri temperaturi okolice. Raziskani so bili vplivi Mo, V, Nb, Ti, Zr ter njihovih karbidov in nitridov na difuzivnost vodika in pridobljeni podatki o številu in vezni energiji pasti. Te nastanejo zaradi napetostnih polj okoli velikih atomov legirnih elementov in v okolici njihovih precipitatov.

Za nekatera jekla za cevovode z različno mikrostrukturo, tudi po simulaciji varjenja, sta bila raziskana difuzivnost in ujetje vodika v pasti, povezana z vodikom, induciranim napetostnim korozijskim pokanjem, ki je bilo opredeljeno z nateznimi preizkusi s konstantno hitrostjo iztezanja. Delo preloma se zmanjšuje z večanjem aktivnosti vodika, kar pove, da je mobilni vodik odgovoren za prelom, vodik v globokih pasteh pa ne vpliva na prelomno vedenje jekel.

Ključne besede: železove zlitine, jekla za cevovode, vodik, aktivnost, permeabilnost, difuzivnost, energija preloma

1 INTRODUCTION

Hydrogen in iron is an important and intensively studied system [1-11]. Severe failure can be caused by the hydrogen embrittlement of steels, which appears as: surface blistering; hydrogen-induced cracking (HIC); stress-corrosion cracking (HISCC); classical, weld and stress cracking and hydrogen-environment embrittlement (HEE).

After adsorption and dissociation hydrogen is dissolved from the atmosphere by absorption according to:

$$H_2\ (gas) = 2H\ (dissolved) \qquad (1)$$

and its concentration follows 'Sieverts law'

$$c_H = K_S \cdot (p_{H2})^{1/2} \qquad (2)$$

where c_H [mol/cm^3] is the concentration of dissolved H atoms, K_S is Sieverts constant and p_{H2} [bar] the hydrogen pressure in the environment. The solubility at 1 bar H_2 [10-14] is extremely low at room temperature, just $3 \cdot 10^{-6}$ at %, but it rises with temperature to $1.6 \cdot 10^{-2}$ at% at 900°C in α-Fe. This corresponds to 3cm^3 of H_2 per 100g Fe. In γ-Fe the solubility is a little higher, $2.3 \cdot 10^{-2}$ at% at 900 °C and in the melt c_H is much higher, 0.13 at% at 1540 °C. As a consequence it is dangerous to saturate steels with hydrogen at elevated temperatures, without the possibility for H_2-desorption during cooling. This desorption may be hindered by oxide scales, enamel or zinc coatings; and an oversaturated solution may result in a variety of failures: shatter cracks, flakes, fish eyes, etc.

Hydrogen absorption occurs not only from gaseous hydrogen, but more often from electrolytes, e.g. during pickling or the corrosion of steels. The most important reactions during the corrosion of iron in an acid environment are [15-18]:
the anodic dissolution of Fe (Volmer reaction):

$$Fe + 2\ H^+ = Fe^{2+} + 2\ H_{ad} \qquad (3a)$$

the recombination of adsorbed H (Tafel reaction):

$$2\ H_{ad} = H_2\ (gas) \qquad (3b)$$

and the absorption of H_{ad}:

$$H_{ad} = H(dissolved) \qquad (3c)$$

The interplay of these reactions establishes a hydrogen activity a_H on the metal surface which is strongly affected by inhibitors and promoters in the electrolyte and by the presence of alloying elements and impurities in the metal surface [19-25]. The study of these latter effects was the subject of our studies [26-28]. The hydrogen activity is defined as the hydrogen concentration c_H related to the hydrogen concentration c_H^0 at T = 0°C and at 1 bar H_2

$$a_H = \frac{c_H}{c_H^O} = \left(\frac{p_{H_2}}{p_{H_2}^O}\right)^{1/2} \qquad (4)$$

If the anodic dissolution reaction (3a) is enhanced (e.g. by the presence of sulfur) and/or the recombination reaction (3b) is retarded (e.g. by arsenate) very high hydrogen activities can occur on steel surfaces which cause the severe absorption of hydrogen.

Hydrogen is very dangerous, especially in ferritic steels, since it generally diffuses very quickly to defects, where it exerts its deleterious effects. In fact, the diffusivity of H in pure and undeformed α-iron at room temperature is very high, about $1 \cdot 10^{-4}$ cm²/sec [27-32], this compares with about $1 \cdot 10^{-16}$ cm²/sec for carbon and nitrogen.

Our own careful studies on very pure iron yielded [6,7]:

$$D_H = (5.12 \pm 0.6) \cdot 10^{-4} \exp(-(4.15 \pm 0.3)\text{kJ mol}^{-1}/RT) \qquad (5)$$

The purer and better recrystallized the iron samples the higher were the data obtained, see **Figure 1**. The activation energy is strikingly low: in comparison with about 80 kJ/mol for carbon and nitrogen. This indicates that hydrogen moves through the ferritic lattice as a proton, tunneling through the interstitial sites. Neither grain boundary nor surface diffusion are faster processes. Alloying elements and deformation generally decrease the diffusivity of H in iron and a tremendous number of Arrhenius lines have been published over the years, on hydrogen diffusion in various steels, see **Figure 2** [6,7,33].

The data in **Figure 2** were derived using the assumption that hydrogen concentration and diffusion follow Fick's laws, and for the higher temperature range the data obtained could be approximately extrapolated to equ. (5), whereas the data at lower temperatures are mostly on lower Arrhenius lines and would yield higher activation energies. This diffusion behaviour of hydrogen was treated by McNabb and Foster [33] by applying a trapping model: ie. the hydrogen atoms

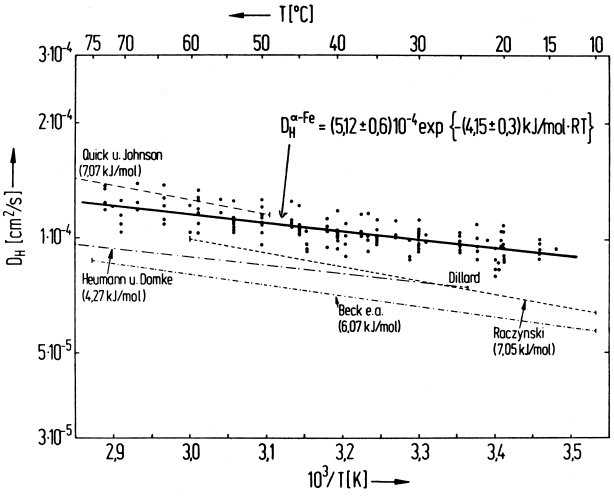

Figure 1: Arrhenius plot of hydrogen diffusion coefficient (D_H) in pure annealed iron, own data [6, 7] and nearby Arrhenius lines from other authors [29-32]

Slika 1: Arrheniusov diagram odvisnosti koeficienta difuzije D_H v čistem žarjenem železu, lastni podatki [6,7] in približne Arrheniusove črte za druge avtorje [29-52]

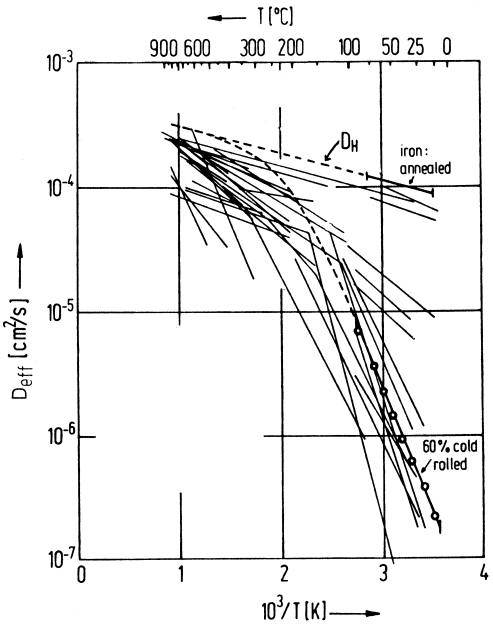

Figure 2: Arrhenius plot of hydrogen diffusivities (D_{eff}) measured by numerous authors in different steels, compared to D_H in pure recrystallized iron, and the H diffusivity in 60% cold-rolled iron which can be described by equation (12) with $N_{ft} = 6.7 \cdot 10^{19}$/cm³Fe and $\Delta H°_{ft}$ = -36 kJ/molH [6, 7]

Slika 2: Arrheniusov diagram odvisnosti koeficienta difuzije D_H po meritvah mnogih avtorjev v različnih jeklih v primerjavi z D_H v čistem rekristaliziranem železu in difuzivnost H v 60 % hladno valjanem jeklu, ki jo opisuje enačba (12) z $N_{ft} = 6{,}7 \cdot 10^{19}$/cm³Fe in $\Delta H°_{ft}$ = -36 kJ/molH [6, 7]

wander in a random manner through the lattice, but tend to get trapped or delayed at sites which act as 'traps'. These sites are regarded as potential wells of greater depth, than those in the undisturbed, defect-free crystal lattice. During the hydrogen diffusion, a local equilibrium is assumed for the 'trapping reaction':

H(in normal, interstitial site) + trap =
= H(in trap) + free normal, interstitial site (6)

This situation corresponds to an adsorption equilibrium where:

rate of adsorption = rate of desorption:

$$k \cdot c_H \, (1-\theta) \cdot N_t = k' \cdot c_t \cdot N \quad (7)$$

where N_t is the number of traps and θ is their degree of occupation, N is the number of normal interstitial sites and $c_t = \theta \cdot N_t$ is the concentration of H in the traps. The quotient of the rate constants for the forward and backward reactions is the equilibrium constant of the trapping reaction (6):

$$\frac{k}{k'} = \frac{\theta \cdot N}{c_H (1-\theta)} = K = \exp(-\Delta G_t^0 / RT)$$
$$= \exp(+\Delta S_t^0 / R) \exp(-\Delta H_t^0 / RT) \quad (8)$$

and for the degree of trap occupation:

$$\theta_t = \frac{c_H \cdot K / N}{1 + c_H K / N} = \frac{\beta}{1+\beta} \qquad \beta = c_H \cdot K/N \quad (9)$$

In steels there are different kinds of traps, in principle a more-or-less continuous spectrum of 'binding energies' $\Delta H_t°$ and values of K is to be expected, however, we usually distinguish between flat traps with
$-\Delta H_{ft} < 30$ kJ/molH and $\beta << 1$ and deep traps with
$-\Delta H_{dt} > 50$ kJ/molH and $\beta >> 1$

The deep traps are already saturated at low values of a_H and c_H and do not affect the diffusivity D_H, whereas the occupation of the flat traps varies with the increase and the decrease of a_H resp. c_H in diffusion experiments or during corrosion.

Non-steady-state diffusion experiments are generally described by Fick's second law, which in the presence of traps describes the H concentration changes in the normal interstitial sites and in the flat traps:

$$\frac{\partial c_H}{\partial t} + \frac{\partial c_{ft}}{\partial t} = D_H \left(\frac{\partial^2 c_H}{\partial x^2} \right) \quad (10)$$

this equation can be rewritten:

$$\frac{\partial c_H}{\partial t} = \frac{D_H}{1 + (\partial c_{ft} / \partial c_H)} \left(\frac{\partial^2 c_H}{\partial x^2} \right) \quad (11)$$

A comparison with the usual formulation of Fick's second law shows that in the presence of flat traps an effective diffusivity of H is observed, which is given by

$$D_{eff} = \frac{D_H}{1 + (\partial c_{ft} / \partial c_H)} = \frac{D_H}{1+\alpha} \quad (12)$$

Since $c_{ft} = \theta \cdot N_{ft}$ we obtain

$$\alpha = K_{ft} \cdot N_{ft} / N$$
$$= (N_{ft} / N) \exp(\Delta S_{ft}^0 / R) \exp(-\Delta H_{ft}^0 / RT) \quad (13)$$

Thus, hydrogen diffusivity decreases with a high occupancy of flat traps N_{ft} and high binding energies $|\Delta H°|$, and the Arrhenius plots, as shown in **Figure 2**, can be explained by the trapping model and equation (12). **Figure 2** also demonstrates that the numerous studies on different steels might well be explained by the effects of strained regions and dislocations [6,7]. The hydrogen diffusivity in iron which has been 60% deformed by cold-rolling corresponds to the diffusion behaviour in many different steels with various degrees of deformation. It is probable that the flat traps correspond to dilated sites near dislocations and the deep traps to dislocation cores. Such dilated sites are also caused by large atoms of alloying elements and by the stresses around precipitates.

Another aim of this study was to clarify the effects of alloying elements such as Ti, Zr, V, Nb, Cr and Mo and their carbides and nitrides on hydrogen solubility and diffusivity, to obtain a better understanding of traps. Studies were conducted on H permeation, diffusion and solubility in several binary alloys of iron and the above mentioned elements, see **table 1** [34-40].

2 EXPERIMENTAL

2.1 Electrochemical Double Cell

Hydrogen absorption, permeation and diffusion were measured using the electrochemical double cell, first described by Devanathan and Stachurski [41,42]. An iron or steel membrane is charged with hydrogen from the entry side, at the exit side the hydrogen is oxidized anodically and the anodic current I_p is a measure of the hydrogen permeation. The schematics in **Figure 3a** demonstrate the principle of the method. Two techniques for hydrogen charging have been applied a) electrolytic charging from an aqueous solution or b) gas-phase charging from pure H_2 or N_2-H_2 mixtures. The application of both techniques us allows to measure at low and high hydrogen activities and at a very well defined standard activity $a_H = 1$, corresponding to $pH_2 = 1$ bar.

For the study of the compositional or structural effects of H absorption, the entry side remained uncoated; this was also the case for sufficiently high cathodic polarisation currents, obtained at constant cathodic current densities i_C or cathodic potentials E_C. Otherwise, especially in the case of hydrogen absorption from the gas phase, the entry side of the membrane had to be Pd coated, to avoid the inhibition of hydrogen adsorption and absorption by oxide films. The exit side of the membrane was always coated with Pd, and polarised anodically at $E_a = 200$ mV(SHE) in a 0,1N

NaOH solution, deaerated by bubbling with N_2. Here the hydrogen is oxidized immediately and its concentration is virtually zero. The anodic permeation current (I_p) is corrected by a blind current, measured when no hydrogen was charged.

2.2 Determination of the permeation coefficient

The permeation coefficient is the product of the hydrogen solubility at 1 bar H_2 and the hydrogen diffusivity in a steady-state experiment:

$$\Phi^0 = c_H^0 \cdot D_H \qquad (14)$$

Its value was determined for each material investigated by charging the Pd-coated membrane from the atmosphere, i.e. pure hydrogen at 1 bar. After attaining a steady state, the flow of hydrogen (j_H) is given by Fick's first law:

$$j_H = D_H \frac{c_H^0 - c_H^e}{d} = D_H \cdot c_H^0 / d = \Phi^0 / d \qquad (15)$$

where d is the membrane thickness; the hydrogen concentration at the entry side ($c_H°$) and at the exit side (c_H^e) = 0. The anodic oxidation of the flux of hydrogen arriving at the exit side yields the permeation current:

$$I_p = j_H \cdot F \cdot A \qquad (16)$$

where F is the Faraday constant and A is the area of the membrane. The permeability results from:

$$\Phi^0 = \frac{I_p \cdot d}{F \cdot A}\left[\frac{mol}{cmsec}\right] = c_H^0 \cdot D_H \qquad (17)$$

2.3 Measurement of hydrogen activity

In electrolytes, hydrogen activitiy on iron and steel surfaces is the result of an interplay of electrochemical reactions (3). The value of a_H can be very high due to the promotion of reaction (3a), the discharge and H adsorption, or to the inhibition of reaction (3b) - the H recombination (Tafel) reaction. It is of great scientific and technical interest to know about effects of the electrolyte and of the steel composition on the established hydrogen activity, e.g. during pickling or corrosion. In this study, permeation measurements were used to obtain the hydrogen activity (a_H) during corrosion in 1 M H_2SO_4.

The hydrogen concentration (c_H) at the entry side of the corroding membrane is determined using:

$$c_H = \frac{I_p \cdot d}{F \cdot A \cdot c_H^0 \cdot D_H} \qquad (18)$$

and related to the hydrogen concentration $c_H°$ at $a_H = 1$ (p_{H2} = 1 bar) by:

$$a_H = \frac{c_H}{c_H^0} = \frac{I_p \cdot d}{F \cdot A \cdot c_H^0 \cdot D_H} = \frac{I_p \cdot d}{F \cdot A \cdot \Phi^0} \qquad (19)$$

Thus, the hydrogen activity can be obtained if the permeation coefficient $\Phi°$ is known from the experiment described above, and $\Phi°$ must be determined separately for each material, since its value is dependent on the steel composition and microstructure.

2.4 Determination of Hydrogen Diffusivity

Upon charging or discharging the membrane in the electrochemical double cell, current transients are observed (see **Figure 3b**). These transients correspond to the absorption of H into the material during charging and the emptying by anodic oxidation during discharging. The process does not only involve the hydrogen in ideal solution, i.e. in the normal interstitial lattice sites, but also the flat traps are filled and emptied, whereas the deep traps are saturated in the very first charging step (see **Figure 3b**) and H sticks to these traps during

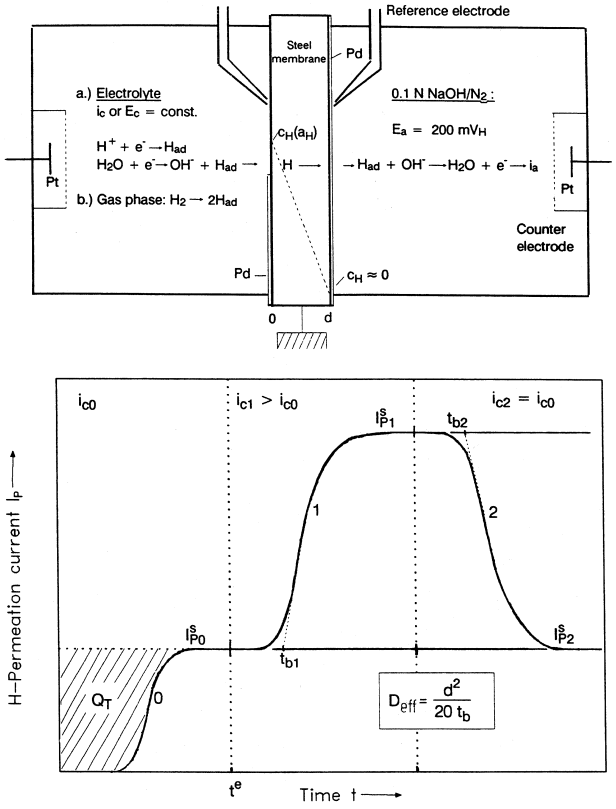

Figure 3: Schematics of measurements in the electrochemical double cell: a) schematic drawing of the double cell, hydrogen charging from the left side, from electrolyte or gas phase, anodic oxidation of the permeating hydrogen in the right cell - measurement of the permeation current I_P; b) schematic presentation of a permeation experiment, in the first step saturation of the deep traps at low charging current i_C and low hydrogen activity a_H, then transients of hydrogen permeation for determination of the effective diffusivity D_{eff}

Slika 3: Shema meritev v dvojni elektrokemični celici: a) Shema dvojne celice, nasičenje z vodikom z leve strani iz elektrolita ali iz plina, anodna oksidacija permeatiranega vodika v desni celici - meritev toka permeacije I_p; b) Shema poskusa permeacije, v prvi stopnji nasičenje globokih pasti pri majhnem toku i_c in majhni aktivnosti vodika a_H, nato tranzienti permeacije vodika za določitev dejanske difuzivnosti D_{eff}

long-term discharging. In our experiments for determining the hydrogen diffusivity the deep traps were always saturated in the first charging step at a low charging current (i_C) and hydrogen activity (a_H) and then the transients of charging and discharging were measured. These non-steady-state experiments lead to a D_H for pure and undeformed iron, and according to equation (12), to a D_{eff}, which is affected by the flat traps. Such a measurement is demonstrated in **Figure 3b**, where the permeation current during a sequence of galvanostatically controlled charging steps is plotted schematically. In the first step at $(i_C)_O$ a low hydrogen activity is established on and in the material and all the deep traps are saturated. Then the cathodic current is raised and lowered at a higher level, in the range of i_C and a_H, where the flat traps can be occupied and released. The permeation transients obtained in that range are described by a series

$$\frac{I_p(t) - I_p^S}{I_p(0) - I_p^S} = 2\sum_{n=1}^{\infty} (-1)^{n-1} \exp(-n^2 \pi^2 \tau) \qquad (20)$$

where $\tau = D_{eff} \cdot t / d^2$. For the determination of D_{eff} from the breakthrough time (t_b) (see **Figure 3b**), the first three terms of the right hand side of equation (20) are used to give:

$$D_{eff} \approx d^2 / 20 \cdot t_b \qquad (21)$$

The breakthrough time is defined by the intersection point of the time axis with the tangent drawn at the inflection point of the permeation curve (see **Figure 3b**).

In the first charging of a hydrogen-free sample, all the flat and deep traps are effective and the diffusivity is not defined. The trapping effect of a steel is characterized by the retention of the permeation through the membrane, i.e. the 'time-lag' till the hydrogen appears at the exit side after the start of charging. A measure for the amount of hydrogen trapped is the charge Q_T corresponding to the hatched area in **Figure 3b**, which can be obtained by the integration of the permeation curve $I_p(t)$ to t_e.

If the hydrogen concentration at the entry side is kept constant, the trapping effect is described by:

$$t_T = 2Q / I_p \qquad (22)$$

For pure trap-free iron

$$t_L = 2Q / I_p = d^2 / 6\, D_H \qquad (23)$$

where D_H is the hydrogen diffusivity in iron without a significant trapping effect.

The theory of McNabb and Foster leads to an expression describing the retardation of hydrogen diffusion by the action of flat traps using equations (12) and (13).

Thus from the non-steady-state permeation curves the number of flat traps (N_{ft}) can be determined. The binding energy of the hydrogen atoms in the flat traps and their concentration can be obtained using equation (12) for calculating D_{eff} from measurements at different temperatures. (This evaluation leads to a value for ΔH_{ft}^0, and ΔS_{ft}^0 is assumed to be small).

From time-lag measurements the effect of deep traps can be derived using the theory of McNabb and Foster [33] which leads to the expression:

$$\left(\frac{t_T}{t_L} - 1\right) = \frac{3\alpha_{dt}}{\beta_{dt}}\left(1 + \frac{2}{\beta_{dt}} - \frac{2}{\beta_{dt}^2} \cdot \ln(1+\beta_{dt})\right) + \alpha_{ft}$$

$$\text{with } \alpha_{dt} = N_{dt} \cdot K_{dt} / N \qquad \beta_{dt} = c_H \cdot K_{dt} / N \qquad (24)$$

Measurements of the time lag as a function of the hydrogen pressure can be fitted according to equation (24) and yield the number of deep traps and the binding energy, in this case ΔG_{dt}^0 is obtained. The value of α_{ft} for the flat traps must be known from non-steady-state measurements of the permeation transients in a range of elevated a_H [40].

3 RESULTS

3.1 Effects of C, S, P, Mn, Si, Cr, Ni, Sn and Cu on corrosion and H absorption

During the pickling of steels hydrogen is often absorbed which may cause defects and failures in the material. The hydrogen absorption is affected by components in the electrolyte, but also by the composition of the steel surface on which alloying elements and impurities may be enriched after hot rolling or after some dissolution in the pickling acid. The retarding effects of Cu on corrosion and H-absorption have been reported [21,22]. Phosphorous is reported to enhance the corrosion and H absorption, while H absorption [19,20,21] is also increased by S, Se, As, Sb and Sn [19,23,24,25]. These effects have been investigated quantitatively for various binary Fe alloys (see **table 1**), using the electrochemical double cell [26,27].

Table 1: Compositions (wt%) of investigated alloys (only main alloying addition, otherwise relatively pure, see original papers)
Tabela 1: Sestava (mas.%) raziskanih zlitin (samo glavni legirni elementi, sicer čiste zlitine, glej izvirne članke)
Binary alloys/Binarne zlitine [26-28]
Fe-0.20 C, Fe-0.046%S, Fe-0.052%P, Fe-0.1%P, Fe-3.08%Si,
Fe-1.53%Mn, Fe-5.19Cr, Fe-10.4%Cr
Fe-5.07%Ni, Fe-10.2%Ni, Fe-0.55%Cu, Fe-3.4% Cu, Fe-0.17%Sn
Fe-0.21%Ti, Fe-0.19%V, Fe-0.3%Zr, Fe-0.35%Nb, Fe-0.36%Mo
Ternary alloys/Ternarne zlitine [34-40]

alloys Fe-Me-C	% Me	% C	alloys Fe-Me-N	% Me	% N
Fe-Ti-C	0.22	0.074	Fe-Ti-N	0.18	0.042
Fe-V-C	0.19	0.081	Fe-V-N	0.20	0.048
Fe-Zr-C	0.27	0.067	Fe-Zr-N	0.63	0.081
Fe-Nb-C	0.35	0.066	Fe-Nb-N	0.35	0.043
Fe-Mo-C	0.33	0.065	Fe-Mo-N	0.37	0.061

For the determination of the hydrogen activities and concentrations established during corrosion the

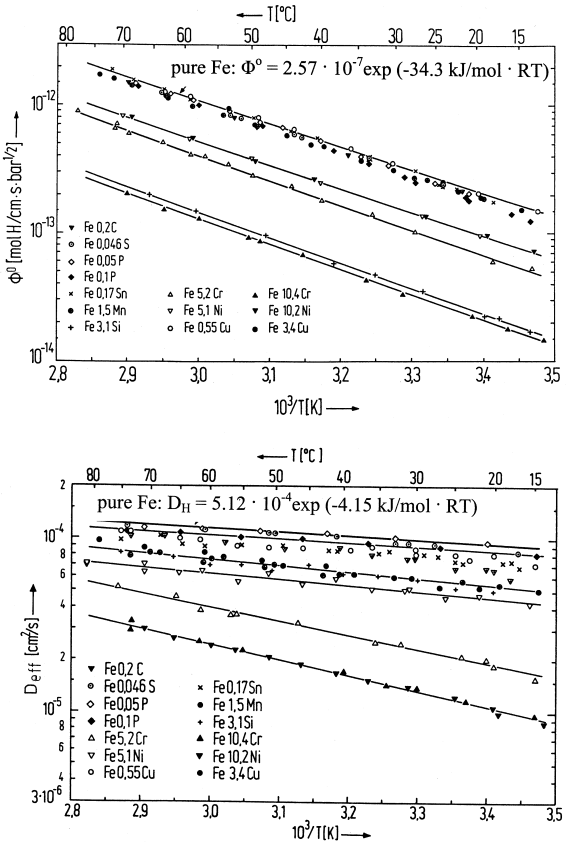

Figure 4: Hydrogen permeation and diffusion in binary Fe alloys [26]: a) permeation coefficient Φ° measured at pH_2 = 1 bar, b) hydrogen diffusivities D_{eff} measured after saturation of the deep traps

Slika 4: Permeacije in difuzija vodika v binarnih zlitinah železa [26]: a) koeficient permeacije Φ°, izmerjen pri pH_2 = 1 bar, b) difuzivnost vodika D_{eff}, izmerjena po nasičenju globokih pasti

permeation coefficient Φ° had to be measured. **Figure 4a** shows that most of the alloying elements cause only a slight reduction in Φ°: the greatest effect was observed for 3,1 wt%Si and 10,4%Cr. For these alloys the H diffusivities were also determined, see **Figure 4b**. Most elements have only a small effect on the diffusivity, but Cr clearly retards H diffusion, indicating trapping by Cr atoms. A calculation of the hydrogen solubility is possible from $c_H = \Phi^0 / D_{eff}$, and the data for the Fe-Si alloy render a clearly decreased solubility [26]. The studied alloying and impurity elements affect H permeation only weakly, Si and Cr decrease the permeation flow, Cr traps H and thus decreases D_H, and Si tends to decrease the H solubility.

The investigated iron alloys, see **table 1**, were corroded in 1M H_2SO_4 and analyzed afterwards by taking AES sputter profiles [27]. Carbon and sulfur are enriched in the surface after corrosion, as is phosphorus, which according to XPS spectra is present as both phosphide and phosphate. In contrast, silicon and chromium are depleted near the surface, these elements are obviously dissolved preferentially. Of the nobler elements, Ni is not clearly enriched, but minor dissolution of Sn and Cu leads to the enrichment of these elements. Current density potential curves measured on these binary alloys in 1M H_2SO_4 indicate, by their shift after some time of corrosion, if anodic or cathodic reactions are changed by these enrichments [28], see **Figure 5**. The most interesting data are the mass loss by corrosion, and the hydrogen activity established during corrosion, which have been recorded after periods of corrosion in 1M H_2SO_4 at 25 °C, see **Figure 5**. The data show a strong increase in corrosion by S and P, whereas Ni, Sn and Cu reduce the amount of corrosion, the other elements have minor effects. The high mass loss of the Fe-Mn alloy was obviously due to its relatively high S content (80 wt.ppm compared to 20 wt.ppm in the unalloyed Fe). The effects of S and P are most probably caused by the catalytic effects of sulphide and phoshide anions on the anodic dissolution of iron. Detailed studies have been conducted on the effects of Cu [18] and of P [34].

The total hydrogen content of the samples after different periods of corrosion in 1 M H_2SO_4 was determined by chemical analysis (hot extraction). The H content of the pure Fe and the Fe-C, Fe-Ni and Fe-Cu alloys are low, around the detection limit of the method ($0.4 \cdot 10^{-6}$ mol H/cm^3). The hydrogen content is enhanced in the Fe-Cr alloys due to the trapping effect. For some alloys the H content during corrosion in 1 M H_2SO_4 goes through a maximum and then decreases, e. g. for Fe-Sn caused by increasing Sn enrichment, and for Fe-P by the formation of a phosphate film. Most striking is the high H content of the Fe-S alloy.

At high values of a_H the amount of hydrogen in Fe and its alloys increases more than the hydrogen activity,

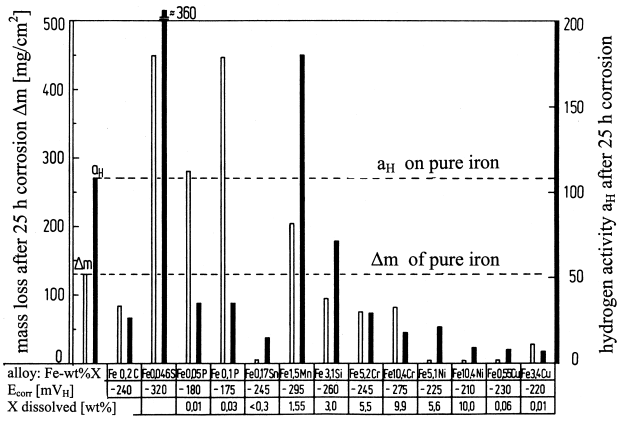

Figure 5: Results of corrosion experiments in 1 M H_2SO_4 at 25 °C on binary Fe alloys [27], mass loss (Δm) and hydrogen activity (a_H) after 25 hours corrosion, corrosion potential and amount of dissolved alloying element (related to the initial composition, not determined for Fe-0.2C and Fe-0.046S)

Slika 5: Rezultati korozijskih poskusov na binarnih Fe-zlitinah v 1 M H_2SO_4 pri 25 °C [27], izguba mase Δm in aktivnost vodika po 25 urah korozije, korozijski potencial in količina raztopljenih legirnih elementov (glede na začetno sestavo, ni določena za Fe-0,2 C in Fe-0,046 S).

Table 2: Data on permeation, diffusivity, solubility and trapping of H in ternary alloys
Tabela 2: Podatki o permeaciji, difuzivnosti, topnosti in ujetju H v ternarnih zlitinah

Alloy	$\Phi^\circ \cdot 10^{13}$ mol/cm · s	Deff · 10^6 cm^2/s	$c_H^{eff} \cdot 10^8$ mol/cm^3	$c_H^{total} \cdot 10^6$ mol/cm^3	$N_{ft} \cdot 10^3$ mol/cm^3	$-\Delta H_{ft}$ kJ/mol	$N_{dt} \cdot 10^6$ mol/cm^3	$-\Delta G_{dt}$ kJ/mol
Fe-Ti-C	1.28	0.72	3.5	10	28	20.6	10	58.5
Fe-Ti-N	2.2	6.1	4.1	1.9	3.0	20.7	1.9	60.5
Fe-V-C	2.12	3.5	7.2	1.8	22	17.2	1.8	57.0
Fe-V-N	2.15	2.7	9.2	3.0	14	18.9	3.1	56.0
Fe-Zr-C	2.05	24	1.1	0.4	0.83	19.9	0.4	58.5
Fe-Zr-N	2.09	3.0	8.5	16	7.3	20.4	17	56.1
Fe-Nb-C	2.16	0.82	30	13	60	18.3	13	56.0
Fe-Nb-N	2.23	5.3	4.7	3.5	9.2	18.2	3.7	54.9
Fe-Mo-C	2.0	42	0.6	0.05	4.0	13.9	0.045	56.5
Fe-Mo-N	1.68	0.27	0.92	0.04	0.9	19.3	0.035	56.0
Fe(60% def,)	2.51	96	26		0.72	27.9	0.62	55.5

due to the formation of dislocations, defects and microcracks.

3.2 Effects of Mo, V, Nb, Ti, Zr and their carbides and nitrides on H diffusivity and solubility

Fine-grained microalloyed steels have found many applications because of their good mechanical properties, high strength and good ductility, but they are susceptible to hydrogen embrittlement. Their microstructure is stabilized by finely divided carbides, nitrides and carbonitrides of the elements V, Nb and Ti, which pin grain boundaries and dislocations. These precipitates generate a lot of extended sites which are suitable for hydrogen atoms, i.e. hydrogen traps. Such traps affect the solubility and diffusivity of hydrogen. To study the effect of the alloying elements Me used in microalloyed steels and their carbides, binary Fe-Me and ternary Fe-Me-C and Fe-Me-N melts were prepared with about 0,2 at.% Me = Mo, V, Nb, Ti, Zr, see **table 1**. The ingots were forged and solution annealed at high temperature. The binary alloys were heat treated at 750 °C for 30 min, the ternary alloys for 300 h at 600 °C.

The materials were characterized by optical and electron microscopy [35-40]. In the Fe-Mo-C alloy, besides the coarse primary Fe_3C-Mo_7C_3 carbides, there were fine Mo_2C needles in the bulk which cause strains and dislocations in their neighbourhood due to their hexagonal structure and incoherence with the iron lattice [34-36]. In contrast, the fine VC_x particles in Fe-V-C alloy are finely dispersed, they are cubic and semicoherent with the Fe lattice and cause less strains. The cubic TiC, NbC and ZrC particles were less numerous and relatively coarse, due to their low solubility. The nitrides are even less soluble and during the solution annealing much less dissolution of the primary nitrides takes place, so that there are less finely dispersed nitride precipitates than carbide precipitates formed after the heat treatment [40].

For these alloys it was most interesting to see, how the alloying elements and their carbides and nitrides affect the diffusivity and solubility of hydrogen by the various different traps generated by the presence of the elements and their precipitates.

For the binary Fe-Me alloys the steady-state permeation measurements produced data for Φ° which are a little lower than for pure iron, the temperature

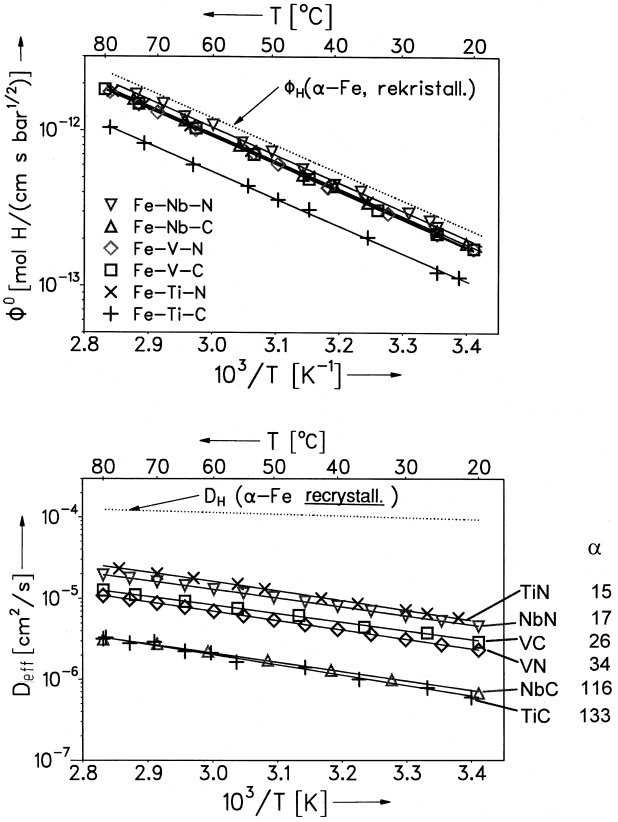

Figure 6: Hydrogen permeation and diffusion in ternary Fe alloys with precipitates of Ti-, V- and Nb carbides and nitrides [40]: a) permeation coefficient Φ° from steady-state experiments, b) hydrogen diffusivities from non-steady-state experiments
Slika 6: Permeacija in difuzija vodika v ternarnih Fe-zlitinah z izločki Ti-, V- in Nb- karbidov in nitridov [40]: a) koeficient permeacije Φ° za poskuse v stacionarnem stanju, b) difuzivnost vodika iz poskusov v nestacionarnem stanju

Table 3: Compositions (wt%) of investigated steels [46]
Tabela 3: Sestava (mas.%) raziskanih jekel [46]

Steel	C	Si	Mn	P	S	Mo	Ni	Cr	Cu	V	Nb
St 0	0.05	0.45	1.45	0.009	0.001	0.007	0.23	0.03	0.3	0.035	0.047
St 1 - 4 similar, different thermomechanical treatments (see table 4)											
St 5	0.6	0.28	0.83	0.008	>.001		-			-	0.033
St 6	0.04	0.29	1.36	0.009		0.14	0.2			-	0.034
St 7	0.03	0.3	1.28	0.006			-			0.04	0.038
A516	0.188	0.267	1.05	0.008	0.001	0.055	0.2	0.189	0.113	-	-
E355	0.116	0.275	1.34	0.008	0.0005	0.059	0.208	0.1	0.12		0.026
E500	0.069	0.248	1.36	0.0009	0.0001	0.208	0.505	0.147		0.046	-

Table 4: Data on permeation. diffusion. solubility and trapping of H in low-alloy steels
Tabela 4: Podatki o permeaciji, difuziji, topnosti in ujetju H v malo legiranih jeklih

Steel		$\Phi^\circ \cdot 10^{13}$ mol/cm^2·s	Deff · 10^6 cm^2/s	ceff · 10^8 mol/cm^3	ctotal · 10^8 mol/cm^3	Nft · 10^3 mol/cm^3	$-\Delta H_{ft}$ kJ/mol	$N_{dt} \cdot 108$ mol/cm^3	$-\Delta G_{dt}$ kJ/mol
St 0	TM(γ) surface	1.63	10.4	2.34	9.58	0.63	23.0	7.4	58.0
	centre	1.63	16	1.53	8.03	0.86	21.0	7.5	53.2
St 1	TM(γ)	1.65	21.5	1.17	4.22	1.4	19.0	3.2	56.0
St 2	TM(α+γ)	1.58	18.1	1.4	5.9	2.6	18.0	5.0	54.0
St 3	TM(γ) + ACC	1.58	17.6	1.42	6.22	3.1	17.6	6.0	52.0
St 4	Q + T	1.79	10.2	2.44	27.3	0.46	23.9	29.0	53.0
St 5	TM(γ)	1.74	39.4	0.63	6.54	8.1	12.5	6.5	54.3
St 6	TM(γ) + ACC	1.56	26.4	0.94	4.76	4.1	15.6	5.0	51.5
St 7	TM(α + γ) + ACC	1.81	33.2	0.75	6.1	7.5	13.3	6.0	53.8
A 516	normalized	1.51	25.1	0.99	8.2	3.6	16.1	7.5	56.5
E 355	"	1.5	23.5	1.01	7.32	1.0	19.6	6.5	57.3
E 500	Q + T	1.6	14.5	1.71	48.6	5.0	17.0	5.5	53.2
Fe (60 % def.)		2.51	1.4	17.4	75.8	0.72	27.9	62	55.5

dependency corresponded to the value ΔH = 34,3 kJ/molH for pure iron. Also for the ternary Fe-Me-C and Fe-Me-N alloys with carbides and nitrides, Φ° was decreased only by a tortuosity factor see **table 2 and Figure 6a**. This decrease is most probably caused by the reduction in the cross-sectional area free for diffusion, due to the precipitates, and possibly, regions with compressive stresses. The effect on Φ° is low for most of the binary and ternary alloys, the largest effect is for the Fe-Ti-C alloy where a high concentration of particles with sizes 1-5 nm was observed by TEM.

In contrast, the non-steady-state measurements of D_{eff} showed strong effects of the alloying elements as well as of the precipitates. H diffusivity in the Fe-Me alloys decreases strongly with increasing atomic size of the elements in the sequence V, Mo, Ti, Nb and Zr [37]. While the effective diffusivity decreases, the hydrogen solubility increases, both caused by flat traps and extended interstitial sites near the Me substituting atoms. In addition, attractive chemical interactions may occur between these hydride-forming elements and the dissolved H-atoms. The binding energies are between -5 kJ/mol H for V and -21 kJ/mol H for Zr [37].

The effective diffusivity is also decreased in the presence of the carbides and nitrides by about one order of magnitude, see **Figure 6b**, and this effect is explained by flat traps with binding energies in the range -17 kJ/mol H (Fe-V-C) and -21 kJ/mol H (Fe-Ti-C, Fe-Ti-N). The amount of dissolved hydrogen is mainly determined by the presence of deep traps with binding energies between -55 kJ/mol H (Fe-Nb-N) and -60.5 kJ/mol H (Fe-Ti-N). The number of flat traps is much higher 10^{-2} - 10^{-3} mol/cm^3 compared with 10^{-6} - 10^{-5} mol/cm^3 of deep traps. However, analysis of the data shows that most of the hydrogen is in the deep traps (> 96%), the concentration in the flat traps is much smaller (1-4 %), and the ideally dissolved hydrogen is much less (< 0,1 %). This is valid at a_H = 1, however, the amount of mobile H in ideal solution and in flat traps increases in proportion to a_H and becomes greater than the amount of H in deep traps at the critical high values of a_H > 100.

Upon corrosion in 1 M H_2SO_4 at 25 °C the alloying elements from the binary Fe-Me alloys are dissolved without enrichment at the surface, as observed with AES. Mo and Zr cause small reductions of cathodic hydrogen formation and corrosion current. The carbides show some corrosion resistance and appear to be enriched in a surface oxide film and also have minor effects on the corrosion behaviour. Mass loss and hydrogen activity established at the corrosion potential

do not differ significantly from the values for pure iron, however, the amount of hydrogen dissolved is considerably enhanced by the alloying elements: in the sequence Mo < V < Nb < Ti < Zr and also for the Fe-V-C alloy with the finely distributed vanadium carbides and the large number of traps.

3.3 Effects of microstructure in pipeline steels

Various low-alloy steels, such as those used for pipelines, were investigated in terms of hydrogen permeation, solubility and diffusion [46], they had different contents of microalloying additions, V and Nb, and were processed differently see **tables 3 and 4**.

In the first series of experiments all the investigated steels were charged with hydrogen from the gas phase at pH_2 = 1 bar and 25 °C, the permeation current was followed until it reached the steady-state permeation current I_p, this measurement yields the amount Q of H absorbed in the steel and the permeation coefficient $\Phi°$, which was determined for the temperature range 10-80 °C.

The data for the commercial pipeline steel St0 show no clear differences for samples taken from the centre and the more deformed surface region, also heat treatment at 240 °C for 80 h had no notable effect on $\Phi°$. Furthermore, the effect of different thermomechanical treatments on $\Phi°$ is small, see **table 4**. In all cases, the decrease of $\Phi°$ compared to pure iron can be largely explained by the effect of the Si content. Silicon decreases the H solubility and thus causes a decrease in $\Phi°$ (see chapter 3.1).

The effects of microalloying elements on $\Phi°$ decrease in the sequence V > Ti > Nb, they are caused by the precipitation of carbides. The small VC_x particles are very finely dispersed, VC_x and TiC are precipitates coherent with the iron matrix, both cause internal stresses and these effect a decrease of $\Phi°$. Internal stresses also result from fast cooling after welding, thus welding simulation also causes a decrease in $\Phi°$. Since the temperature dependence of $\Phi°$ in all cases can be described by the activation energy valid for pure iron 34,3 kJ/molH, the effects described are just decreasing the temperature-independent factor, and can be explained by the reduced cross-section of permeation, as affected by the carbides and by compressive stresses.

The diffusivity D_{eff}, as affected by the flat traps, shows much stronger deviations from the ideal value for pure iron than the permeation coefficient see **table 4**. D_{eff} is decreased by increasing trap density, especially in the range of higher temperatures, and a higher binding energy causes a steeper decrease mainly in the range of lower temperatures. The effect of high binding energies is observed to correlate with high dislocation densities and internal stresses. This is true for the steels investigated in this study, in the case of the strongly deformed near-surface region of the pipeline steel St 0 and after different thermomechanical treatments, and for the heat-affected zones (HAZ), especially after very rapid cooling from high temperatures. By tempering, the quenching effect can be partially removed, but only if the microstructure is not stabilized by fine carbide dispersions. Especially the finely dispersed VC_x precipitates, which are able to stabilize a dislocation network and cause a relatively low value of D_{eff}, more-or-less independent of heat treatments and welding simulations.

The concentration of mobile hydrogen, which is effective in diffusion and steady-state permeation is high for the steels with high dislocation densities and internal stresses. This is demonstrated for the samples from the surface region of the pipeline steel, for the quenched and tempered steels (St4, E500) and for the various HAZ structures after welding simulation. The disordered microstructures are stabilized again, more or less, by the carbide formers Ti, Nb and especially V (HAZ structures). Tempering decreases the internal stresses and simultaneously the trapping effect and hydrogen concentration c_H^{eff} are reduced. Only the presence of V stabilizes these data.

Information on the deep traps was obtained from time-lag measurements according to equation (24), from fitting plots of $(t_T - t_L)/t_L$ vs. $(p_{H2})^{-1/2}$. The trapping by deep traps is enhanced for steels which were tempered after a quench, i.e. quenched and tempered steels and HAZ structures. For the base steel without Ti, Nb and V this effect is not observed, and we may conclude that the number of deep traps is connected to the presence of carbide precipitates. Obviously, the number of deep traps increases with the increasing number of carbide/ferrite interfaces and for incoherent precipitates. Titanium causes large effects with deep traps, due to the incoherence of TiC. Besides the effects of carbides, deformation also leads to an increased number of deep traps.

The effect of deep traps depends on their number and on the binding energy. The latter influence is minor, since even at the hydrogen activity a_H = 1, the saturation of traps with ΔG = -51 kJ/mol is already 73%, at a_H = 10 it is 96 %. The values found for the investigated steels are between -51 and -58 kJ/mol H, and thus very near to the value determined for pure iron with a high deformation and dislocation density: -55.5 kJ/molH. In the literature, values of -59 to -60 kJ/molH are given for deep traps in dislocations and grain boundaries [8]. Therefore, we can conclude that deep traps at, or in the neighbourhood of, carbides are just extended interstitial sites, as in dislocation cores and grain boundaries. Special chemical interactions of H with carbides and also with nitrides are improbable, and high binding energies of -90 kJ/mol H to TiC [43,44] are not confirmed by our work.

The total hydrogen content is the sum of the hydrogen in deep traps and the mobile hydrogen. The

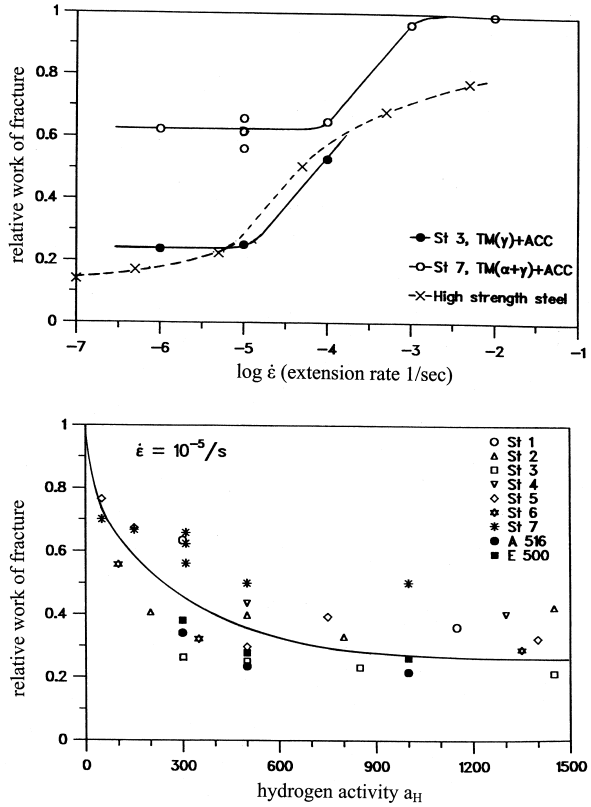

Figure 7: Results of constant-extension-rate tests (CERT) with several pipeline steels [46] in electrolyte 1 M H_2SO_4 + 10^{-3} M As_2O_3 under cathodic charging with hydrogen; relative fracture energy dependence on a) the extension rate $\dot{\varepsilon}$ at a_H = 300, b) the hydrogen activity a_H

Slika 7: Rezultati poskusov s konstantno hitrostjo iztezanja (CERT) na več jeklih za cevovode [46] v elektrolitu 1 M H_2SO_4 + 10^{-3} As_2O_3 pri katodnem nasičenju z vodikom; relativna energija preloma v odvisnosti od: a) hitrosti iztezanja $\dot{\varepsilon}$ pri a_H = 300, b) aktivnosti vodika a_H

latter is in ideal solution and in flat traps, and its concentration is approximately proportional to a_H. In pure recrystallized iron and steels with low strength, at high a_H sources of dislocations become active and new dislocations are generated [45]. For the ternary alloys Fe-V-C and Fe-Ti-C with maximum strength ~ 350 MPa the trap density was increased above a_H = 30, and the total H content determined by permeation study and by hot extraction were about equal. The formation of dislocations and traps will need higher hydrogen activities, a_H > 70 for fine-grain steels with higher strength. For lower values of a_H the total H content can be satisfactorily calculated from the permeation data. Such a calculation shows that at a_H = 1 the hydrogen in deep traps prevails, whereas at the higher values of a_H > 70 the amount of diffusible H becomes higher for all the investigated steels.

3.4 Fracture behaviour in the presence of hydrogen

The effect of hydrogen on the fracture of the investigated steels (in **table 3**) was observed in constant-

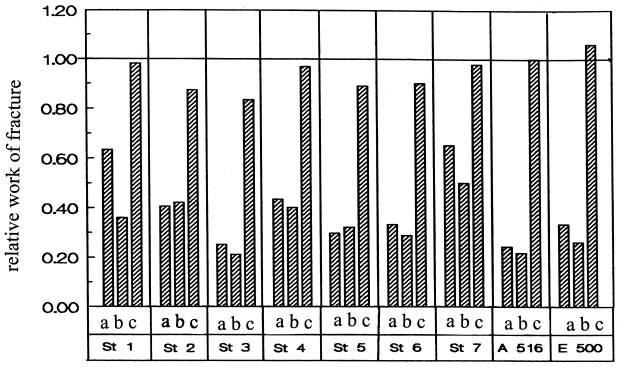

Figure 8: Relative fracture energies of some pipeline steels from constant-extension-rate tests (CERT) [46] at $\dot{\varepsilon}$ = 10^{-5}/s: a) CERT in electrolyte at $a_H \approx 500$, b) CERT in electrolyte at $a_H \approx 1000$ - 1500, c) CERT in air after 96 h precharging and 24 h hydrogen desorption at room temperature

Slika 8: Relativna energija preloma nekaterih jekel za cevovode, določena s poskusi s konstantno hitrostjo iztezanja (CERT) [46] pri $\dot{\varepsilon}$ = 10^{-5}/s: a) CERT v elektrolitu pri $a_H \approx 500$, b) CERT v elektrolitu pri $a_H \approx$ 1000-1500, c) CERT v elektrolitu po 96 urah katodnega nasičenja in 24 urne desorpcije vodika pri sobni temperaturi

extension-rate tests (CERT), conducted in: 1 M H_2SO_4 + 10^{-3}M As_2O_3, at charging currents $-i_C$ = 0.1 to 8 mA/cm^2. The hydrogen activities could be established between a_H = 50 and 1500, as was derived from the dependence of a_H on i_C which was determined before by permeation studies. As a measure of the effect of H on the mechanical properties of steels, the decrease of the work needed for fracturing the steels was measured, i.e. the relative work of fracture

$$W_f = (W/R_m)(W^0/R_m^0) = W_f / W_f^0 \qquad (25)$$

where R_m is the maximum tensile strength, R_m^0 without hydrogen.

At first a study was conducted on the effect of extension rate $\dot{\varepsilon}$ in tests on specimens which were not precharged with H. The processes leading to the hydrogen effects, H diffusion and local accumulation, H-induced crack formation and crack growth need some time, therefore the extension rate $\dot{\varepsilon}$ must be low enough to realize the hydrogen effects. The results indicate that a rate lower than 10^{-5}/sec should be used to obtain reliable data for W_f, see **Figure 7a**. Another important result was obtained in tests with different steels at various values of a_H, as established by varying the charging current i_C. The work of fracture W_f decreases with increasing a_H, but at values a_H > 500, W_f remains largely constant. Small differences in the hydrogen susceptibility of the steels can be seen from the data in **Figure 7b**.

In addition, a series of tests were performed under three different conditions:

a) CERT at a_H ~ 500, without precharging;
b) CERT at a_H ~ 1000-1500, without precharging;
c) CERT in air (a_H = 0) after 96 hours precharging at a_H ~ 1200, and 25 h in air at ambient temperature.

Series (a) and (b) gave no clear differences in W_f, see **Figure 8a**, which confirms again that the fracture work becomes independent of a_H above $a_H \sim 500$. Certain differences in H susceptibility can be seen for the different steels, depending on the microstructure.

Most important is the result of the last series (c), which gave values for W_f only a little smaller than the original value $W°_f$ in absence of hydrogen, or even equal to $W°_f$ and higher. While the steels are held in air at room temperature all mobile H will desorb, but the hydrogen in deep traps will stay in the steels. So these experiments clearly prove that it is mainly the mobile H and not the H in deep traps which is responsible for the H effects on fracture.

A welding simulation enhances the susceptibility to H, as shown by the tests on one of the steels treated in two different ways: 1. original state, 2. 1 sec 1250 °C + ΔT(800-500 °C) = 15 sec, 3. 1 sec 1250 °C + ΔT (800-500 sec) = 15 sec + 2 hours 600 °C. Both welding simulations cause a significant decrease in W_f, even tempering at 600 °C does not improve the behaviour.

4 CONCLUSIONS

Knowledge on hydrogen absorption and diffusion in steels is important for understanding defects and cracking caused by hydrogen in steel. Extensive studies have been conducted on iron, binary and ternary iron alloys and steels, using the electrochemical double-cell method, for determing the H permeation, diffusivity, solubility and activity upon charging the specimens from the atmosphere or from an electrolyte.

The effects of the alloying elements C, S, P, Mn, Si, Cr, Ni, Sn and Cu on hydrogen permeation and diffusion have been studied on binary Fe alloys. The permeation coefficient $\Phi° = c_H \cdot D_H$ is considerably decreased by Si and Cr, Si reduces the solubility c_H and Cr reduces the diffusivity D_H by trapping. The surface layer composition after corrosion in 1 M H_2SO_4 was investigated by AES and XPS, Cu, Sn, P and C are enriched after corrosion, Cr is preferentially dissolved. Cu, Sn and Ni inhibit the dissolution and decrease the hydrogen activity during corrosion. S, P and Mn enhance the corrosion attack, and increase the hydrogen activity.

The H diffusivities in Fe alloys and steels are strongly decreased at low temperatures < 200 °C by trapping, i.e. the binding of H to traps at an energy level lower than in the normal interstitial sites. Data on trapping were derived according to the theory of McNabb and Foster [33], from non-steady state permeation studies on binary Fe-Me, ternary Fe-Me-C and Fe-Me-N alloys (Me = Ti, V, Zr, Nb, Mo). For all alloys, flat traps can be found with binding energies around -19 kJ/mol, which are filled to a level more-or-less dependent on a_H and affect the diffusion of the mobile H. In contrast, the deep traps with binding energies around -57 kJ/mol are already filled at low a_H and the hydrogen in deep traps is virtually immobile at ambient temperature. There is no indication of a special chemical bonding of H to carbides or nitrides, it can be assumed that the deep traps are sites in dislocation cores, grain boundaries and at interfaces, whereas the flat traps are extended lattices sites near such defects.

These considerations are also true for low-alloy steels, as shown for some pipeline steels. These steels were tested for their hydrogen susceptibility in constant-extension-rate tests, conducted after charging with hydrogen from an electrolyte. No great differences were observed in the dependence on their microstructure. The work in fracturing at a low extension rate (10^{-5}/sec) decreased with increasing a_H but was about constant at $a_H > 300$. After precharging and desorption of the mobile hydrogen at room temperature there was no effect of the hydrogen in deep traps, on the work of fracture. Only the mobile H in an ideal solution or in flat traps is involved in fracture, its concentration increases approximately in proportion to a_H. Transgranular cracks occur in highly stressed regions after mobile H has concentrated sufficiently. The immobile H in deep traps has no effect on the fracture behaviour of the steels, thus there is no direct correlation between total hydrogen content and the susceptibility to hydrogen-induced cracking and stress-corrosion cracking.

5 REFERENCES

[1] J. D. Fast: Interaction of Metals and Gases, Academic Press 1965, 126-147
[2] R. A. Oriani: Acta Met. 18 (**1970**) 147
[3] R. A. Oriani: Ann. Rev. Matr. Sci. 8 (**1978**) 327
[4] E. Riecke: Arch. Eisenhüttenwes. 44 (**1973**) 647-656
[5] E. Riecke: Werkstoffe u. Korrosion 29 (**1978**) 106-112
[6] E. Riecke: 8th Intern. Congress on Metallic Corrosion, Mainz 1981, Vol. 1, 605-610
[7] E. Riecke: 3rd Intern. Congress on Hydrogen in Metals, Paris, June 7-11, 1982
[8] J. P. Hirth: Metallurg. Trans. 11 A (**1980**) 861
[9] P. Neumann: Stahl u. Eisen 107 (**1987**) 577
[10] H. Gräfen, D. Kuron: Chem.-Ing.-Tech. 59 (**1987**) 555
[11] A. Turnbull (Ed.): 'Hydrogen Transport and Cracking in Metals', The Inst. of Materials, London 1995
[12] M. H. Armbruster: J. Amer. Chem. Soc. 65 (**1943**) 1043
[13] W. Eichenauer, H. Künzig, A. Pebler: Z. Metallkde. 49 (**1958**) 220
[14] H. Schenck, K. W. Lange: Arch. Eisenhüttenwes. 37 (**1966**) 739
[15] J. O'. M. Bockris, A. K. N. Reddy: Modern Electrochemistry 2, Plenum Press, New York 1977
[16] H. Kaesche: Die Korrosion der Metalle, Springer, Heidelberg 1979
[17] E. G. Dafft, K. Bohnenkamp, H. J. Engell: Corros. Sci. 19 (**1979**) 591
[18] C. Kato, H. J. Grabke, B. Egert, G. Panzner: Corros. Sci. 24 (**1984**) 591
[19] J. F. Newman, L.L. Shreir: Corr. Sci. 9 (**1969**) 631
[20] J. Albrecht, H.E. Bühler, S. Baumgartl: Archiv Eisenhüttenwes. 45 (**1974**) 561
[21] H. E. Bühler, S. Baumgartl, W. Warnecke: Archiv Eisenhüttenwes. 46 (**1975**) 811
[22] H. Inagaki, M. Tanimura, I. Matsushima, T. Nishimura: Tans. ISIJ. 18 (**1979**) 149

[23] T. Ramchandran, K. Bohnenkamp: Werkst. Korros. 39 (**1979**) 43
[24] Z. A. Foroulis: Werkst. u. Korros. 31 (**1980**) 463
[25] R. Pöpperling, W. Schwenk: Werkst. u. Korros. 31 (**1980**) 15
[26] E. Riecke, B. Johnen, H. J. Grabke: Werkstoffe u. Korrosion 36 (**1985**) 435
[27] E. Riecke, R. Möller, B. Johnen, H. J. Grabke: Werkstoffe u. Korrosion 36 (**1985**) 447
[28] E. Riecke, B. Johnen, H. J. Grabke: Werkstoffe u. Korrosion 36 (**1985**) 455
[29] W. Beck, J. O'. M. Bockris, J. Mc.Breen, L. Nanis: Proc. Roy. Soc. A 290 (**1966**) 220
[30] Th. Heumann, E. Domke: Int. Meeting on Hydrogen in Metals, Jülich 1972, Vol. II, 492-515
[31] W. Racczynski: Phys. Stat. Sol. (a) 48 (**1978**) K27
[32] N. R. Quick, H. H. Johnson: Acta Met. 26 (**1978**) 903
[33] A. McNabb, P. K. Foster: Trans Metallurg. Soc. AIME 227 (**1963**) 618/27
[34] E. Riecke, R. Möller, B. Johnen: Corros. Sci. 27 (**1987**) 1027
[35] E. Riecke, H. Liesegang, H. J. Grabke: Werkstoffe u. Korrosion 38 (**1987**) 310-316
[36] E. Riecke, H. Liesegang, H. J. Grabke: Werkstoffe u. Korrosion 38 (**1987**) 310
[37] E. Riecke, B. Johnen, H. Liesegang, A. Thoms, B. Reynders, H. J. Grabke: Werkstoffe u. Korrosion 39 (**1988**) 525
[38] E. Riecke, B. Johnen: Werkstoffe u. Korrosion 42 (**1991**) 528
[39] E. Riecke B. Johnen: Werkstoffe u. Korrosion 42 (**1991**) 626
[40] F. Gehrmann, E. Riecke, H. J. Grabke: Effects of the Nitrides and Carbides of V, Nb and Ti on the Diffusion and Dissolution of Hydrogen in Iron, in (11) p. 216-226. see also: Report EUR 16083DE, Europäische Gemeinschaften, Luxemburg 1997
[41] M. A. V. Devanathan, Z. Stachurski: Proc. Roy. Soc. A 270 (**1962**) 90
[42] M. A. V. Devanathan, Z. Stachurski: J. Electrochem. Soc. 111 (**1964**) 619
[43] A. J. Kumnick, H. H. Johnson: Acta Met. 28 (**1980**) 33
[44] G. M. Pressouyre, I.M. Bernstein: Metallurg. Trans. 9A (**1978**) 1571
[45] S. D. Kapusta, T. T. Kam, K. E. Heusler: Z. physik. Chemie N.F. 123 (**1980**) 219
[46] E. Riecke, H. J. Grabke: Einfluß der Mikrostruktur von Stählen auf die Wasserstoffabsorption und wasserstoffinduzierte Rißbildung, Report EUR 16080 DE, Europ. Gemeinschaften Luxemburg 1997